communications physics

ARTICLE

https://doi.org/10.1038/s42005-022-01101-z OPEN

Topological random fractals

Moein N. Ivaki [1,2], Isac Sahlberg[1,2], Kim Pöyhönen[1,2] & Teemu Ojanen [1,2]✉

The search for novel topological quantum states has recently moved beyond naturally occurring crystalline materials to complex and engineered systems. In this work we generalize the notion of topological electronic states to random lattices in non-integer dimensions. By considering a class *D* tight-binding model on critical clusters resulting from a two-dimensional site percolation process, we demonstrate that these topological random fractals exhibit the hallmarks of topological insulators. Specifically, our large-scale numerical studies reveal that topological random fractals display a robust mobility gap, support quantized conductance and represent a well-defined thermodynamic phase of matter. The finite-size scaling analysis further suggests that the critical properties are not consistent with the expectations of class *D* systems in two dimensions, hinting to the nontrivial relationship between fractal and integer-dimensional topological states. Our results establish topological random fractals as the most complex systems known to support nontrivial band topology with their distinct unique properties.

[1] Computational Physics Laboratory, Physics Unit, Faculty of Engineering and Natural Sciences, Tampere University, P.O. Box 692, FI-33014 Tampere, Finland. [2] Helsinki Institute of Physics, P.O. Box 64, FI-00014 Helsinki, Finland. ✉email: teemu.ojanen@tuni.fi

Since the discovery of the quantum Hall effect, the quantized conductance, dissipationless currents and unconventional edge excitations have captured the fascination of generations of physicists[1–4]. These remarkable properties, unlikely from the point of view of traditional solid-state physics, ultimately result from the topology of the electronic spectrum[5]. Recent efforts have revealed that topological states in naturally occurring materials are ubiquitous in nature[6–8].

Currently, the research of topological states of matter has moved beyond crystalline solids to amorphous and quasicrystalline systems[9–36,36–42]. While it is not yet clear whether these states of matter exist in nature, they can be realized in artificial designer systems[43–46,46–49]. Besides offering new avenues for functional devices, these systems open a new chapter in the physics of topological matter and the theory of Anderson localization. In this vein, the possibility of topological states in fractals has stirred a new research direction. Despite reported signatures of topology in a number of fractal lattices, many aspect of these systems remains unclear or controversial[50–62]. The existence of the spectral gap, possibility of supporting quantized responses and anomalous dependence on system details, such as the coordination number and connectivity of lattice sites, remain under debate. Furthermore, since the studies are mostly restricted to modest-size structures without systematic finite-size scaling analysis, it is not clear whether the finite samples actually represent a well-defined thermodynamic phase of matter.

The research on topological fractals so far has been limited to deterministic self-similar structures. The organization principle of these structures, as of quasicrystals, is completely deterministic without any element of randomness. In contrast, in this work we demonstrate a topological phase on fundamentally more complex self-similar random lattices depicted in Fig. 1. These random fractals are *statistically* self-similar, i.e. generated from a probability distribution, and characterized by a non-integer spatial dimension[63,64]. Specifically, we study a symmetry class D Hamiltonian on critical clusters of 2d square lattice percolation. The geometry of the critical percolating cluster is characterized by the fractal dimension $d_f = \frac{91}{48} < 2$ (the number of sites within a circle of radius r scales as r^{d_f} for large r) and a set of standard critical exponents. Our main findings are summarized in the following discoveries: (I) the studied topological random fractals have in general a gapless energy spectrum but exhibit a well-defined mobility gap protecting the topological phase, (II) the studied system supports robust quantized conductance, (III) finite-size scaling analysis show that topological random fractals represent a well-defined thermodynamic phase of matter, (IV) the localization exponent for class D random fractals is incompatible with the universal value $\nu = 1$ in two dimensions. The last property suggests that, despite similarities with topological insulators in integer dimensions where they are embedded, topological random fractals represent a distinct state of matter.

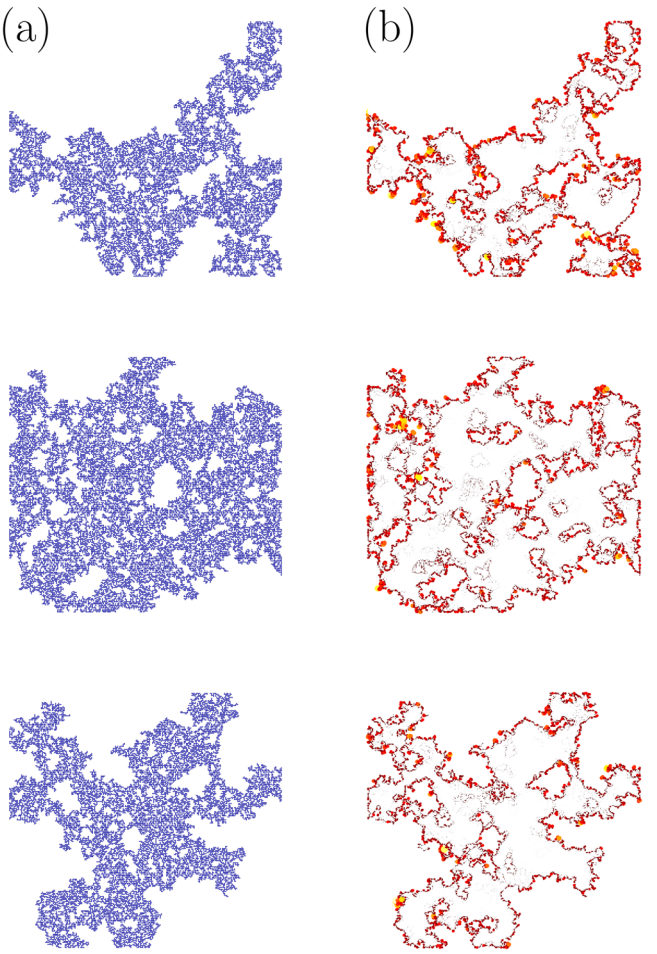

Fig. 1 Critical percolating networks are archetypal examples of random fractals. a Here we see three finite snapshots of critical clusters with linear size $L = 250$ and **b** the local density of states of the studied topological lattice model at the centre of the mobility gap $E = 0$. Despite the seeming absence of clear distinction between the bulk and edge modes, these structures support robust quantized conductance.

Results

Percolation-generated random fractal lattices. Percolation theory provides a paradigmatic framework to study complex systems in physics and many related fields[65–67]. In this work we consider random lattices arising from a site percolation process on a square lattice where each site is randomly occupied by probability p. There exists a critical concentration $0 < p_c < 1$, known as the percolation threshold, above which the random lattice has an infinite nearest-neighbour-connected cluster in the thermodynamic limit. Below the threshold, the system consists of disconnected finite clusters. When approaching the percolation threshold, the characteristic length scale of the lattice $\xi(p)$ (the statistical correlation length) diverges as $\xi(p) \propto |p - p_c|^{-4/3}$, signifying that the percolating critical cluster becomes a scale-free random fractal. The fractal dimension $d_f = \frac{91}{48}$ is universal for both site and bond percolation in two dimensions and it can be derived, for example, from a set of other universal critical exponents[67]. A finite snapshot of a percolating network at $p \neq p_c$ appears indistinguishable from an infinite random fractal up to the correlation length $\xi(p)$.

On a square lattice, the percolation transition takes place at $p_c \approx 0.593$[65,68]. In Fig. 1 we have illustrated three finite-size realizations of the random fractals generated by the percolation process (see "Methods" for details). The properties of the critical percolation clusters have been studied in great detail in various contexts[65]. In striking contrast to all 2d lattices, the fractal spatial dimension of a critical cluster $d_f < 2$ means that they do not have a well-separated bulk interior and boundary. As the topological phases typically manifest in protected edge modes, the absence of clear distinction between the interior and the boundary appears disconcerting. Moreover, despite the statistical self-similarity, random fractals exhibit wild sample-to-sample fluctuations. The complexity of random fractals is underlined by the fact that random fractals differ from deterministic fractals in much the same way as amorphous lattices differ from regular lattices. Remarkably, despite the controversial present understanding of

topology in deterministic fractals, our results establish that random fractals can support robust topological states.

Model and phase diagram. Next we define a two-band tight-binding model[69–71] on critical square lattice percolation clusters. The model is determined by the Hamiltonian

$$\mathbb{H} = (2-M)\sum_i \boldsymbol{c}_i^\dagger \sigma_z \boldsymbol{c}_i - \frac{t}{2}\sum_{<ij>} \boldsymbol{c}_i^\dagger \eta_{ij} \boldsymbol{c}_j - \frac{t_2}{2}\sum_{\ll ij\gg} \boldsymbol{c}_i^\dagger \eta_{ij} \boldsymbol{c}_j + \text{h.c.}, \quad (1)$$

where M is the onsite mass parameter and t and t_2 represent the hopping amplitudes between the nearest- and second-nearest-neighbour sites on a square lattice provided those sites are present in a given random realization. The matrix $\eta_{ij} = \sigma_z + i\cos\theta_{ij}\sigma_x + i\sin\theta_{ij}\sigma_y$ is determined by θ_{ij}, which denotes the angle between the x axis and the bond vector from site i to site j. The two-component operators $\boldsymbol{c}_i^\dagger = (c_{i,1}^\dagger, c_{i,2}^\dagger)$ create fermions at site i, and $\sigma_{x,y,z}$ are the Pauli matrices operating in the two-orbital space. The model (1) breaks time-reversal symmetry and satisfies particle-hole symmetry as $\sigma_x \mathbb{H}^* \sigma_x = -\mathbb{H}$, hence belonging to the symmetry class D[71–73]. On a square lattice in the clean limit, the model supports topological phases with nonzero Chern number. Potentially other symmetry classes may support topology on random fractals as well; the choice to study class D here was made to simplify the large-scale computing efforts, as a minimal model proof-of-concept already poses a substantial computational challenge. In the remainder of this paper, we set $t = 1$ and express the other parameters in units of t. On a regular lattice, a disordered class D model is known to host a metallic phase which separates the two insulating topological phases. In the case of anisotropic models, an intervening localized phase appears. The localization exponents at metal-insulator and insulator-insulator transitions are known to be $\nu_{\text{MI}} \approx 1.4$ and $\nu_{\text{II}} = 1$, respectively[74–80].

Defining a topological phase on a random fractal poses conceptual challenges. While real-space methods for calculating topological invariants exist, the fractal does not lend itself well to these methods. A more critical issue is the fact that the known methods are defined for integer dimensions, and there are indications that they may not carry the same physical consequences on a fractal of dimension $1 < d_f < 2$[53,55,81,82]. It is even unclear presently whether the mathematical structures that underline the topological classification in integer dimensions can be generalized to fractal dimensions. We bypass these delicate issues by focusing on the possibility of quantized two-terminal conductance G, which we adopt as an operational criterion of nontrivial fractal topology. This is physically motivated by the fact that, irrespective of mathematical definitions, a quantized two-terminal conductance carries direct observational relevance. Furthermore, the only mechanism known to result in robust quantized nonzero conductance plateaus in disordered systems is nontrivial topology.

To numerically evaluate G we employ the KWANT software[83], which implements transport calculations using scattering theory[84] (see "Methods"). The resulting conductances are calculated at the half-filling $E = 0$ when not stated otherwise. Figure 2 displays the phase diagram in the (t_2, M) plane obtained by calculation of the configuration-averaged conductance. This reveals the existence of a topological phase, which is characterized by quantized conductance $G = 1$ in the thermodynamic limit, and trivial, insulating regions. As discussed below in the context of finite-size scaling, the topological phase is separated from the trivial phases by a critical line which corresponds to critical

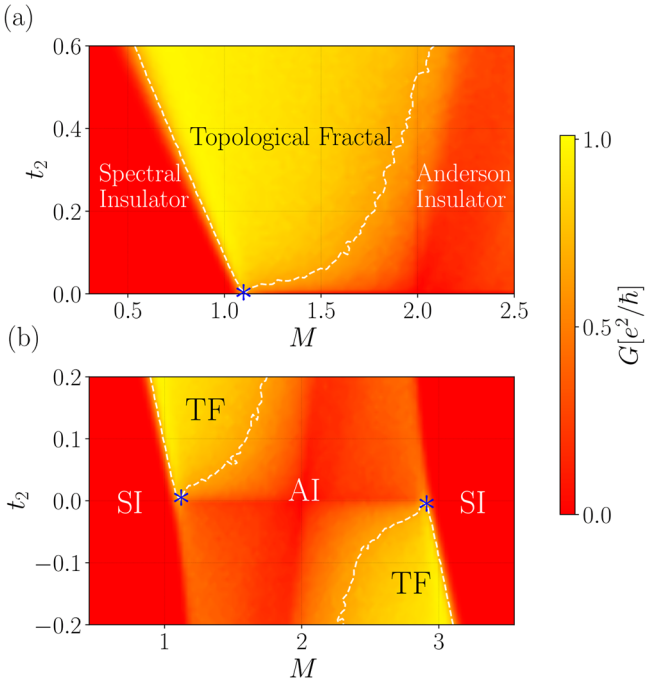

Fig. 2 Topological phase diagram of the random fractals. a Phase diagram of the studied systems as a function of the second-nearest-neighbour hopping t_2 and the mass parameter M, obtained by calculation of the two-terminal conductance G for half-filled square-shaped systems with linear dimensions $L = 150$. The dashed white line represents the approximate critical surface $G^c = 0.65$, which encloses the topological regime where $G \to 1$ in the thermodynamic limit $L \to \infty$. The blue star signifies the tricritical point at $t_2 = 0$ and $M^c \approx 1.1$ and the colour bar indicates the value of G. Data is averaged over 650 independent random realizations. **b** Same as (**a**) but for an extended parameter regime. Here $L = 120$ and data is averaged over 800 configurations.

conductance $G^c \approx 0.65$. The critical point at $(t_2^c, M^c) \approx (0, 1.1)$ signifies a meeting of three distinct phases, the topological phase, a trivial spectral insulator and a trivial Anderson insulator. A finite second-nearest-neighbour hopping $|t_2| > 0$ opens up a robust topological phase studied in detail below. In contrast to the sharp spectral insulator-topological fractal phase boundary, identifying the topological fractal-Anderson insulator phase boundary is complicated in finite-size systems due to the fact that both phases are gapless as seen below. The nature of the transition between the trivial spectral and Anderson insulator phases at the $t_2 = 0$ line is illustrated in Fig. 3. In Fig. 3(a), the mid-spectrum density of states indicates the formation of a spectral gap for $M < 1.1$, while for $1.1 < M < 2.9$ the system is in a gapless Anderson-localized phase. However, both phases separated by the tricritical metallic point $(t_2^c, M^c) \approx (0, 1.1)$ are insulating, as seen in Fig. 3(b). The localization of states in the Anderson insulating phase is further analyzed by the configuration-averaged inverse participation ratio $\text{IPR}(E) = \sum_{i\alpha} |\Psi_{i\alpha}^E|^4$. As can be seen from the inset of the Fig. 3(b), the inverse participation ratio in the region $1.1 < M < 2.9$ shows great enhancement around $E = 0$ everywhere in the Anderson-localized regime, indicating that the spectrum is gapless but consists of trivial localized states.

Topological random fractal phase. Having established the global features of the phase diagram, we now study the properties of the topological random fractal phase in detail. As seen in Fig. 4(a), at the transition point between the spectral insulator and topological

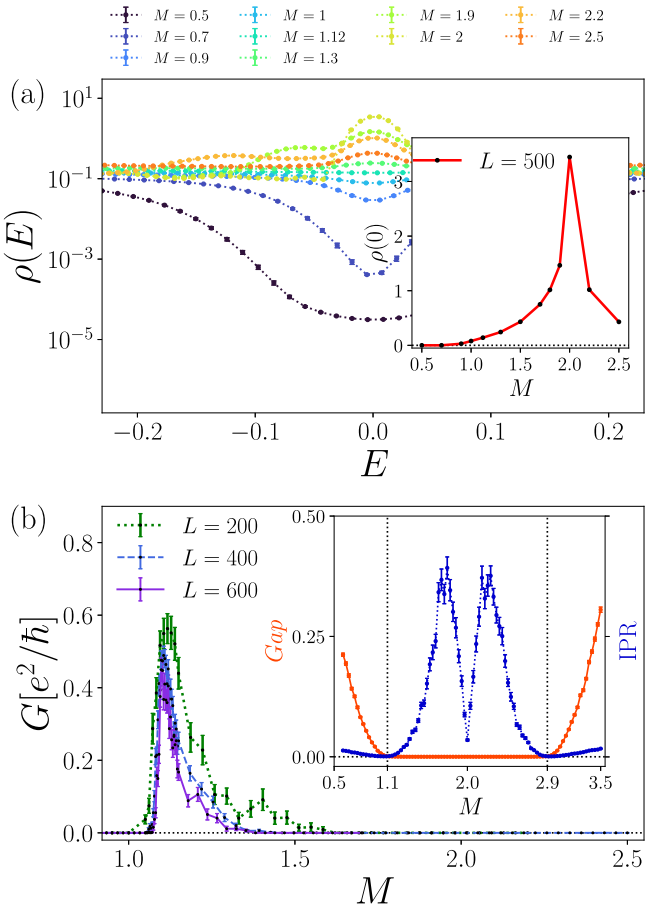

Fig. 3 Spectral insulator-Anderson insulator transition. a Configuration-averaged normalized density of states $\rho(E)$ for the Hamiltonian (1), shown for different mass parameters M at linear system size $L = 500$ with second-nearest-neighbour $t_2 = 0$. Inset shows the behaviour of $\rho(E \approx 0)$ as M is varied. The feature at $M = 2$ originates from a gapless point of the Hamiltonian (1) on a square lattice. **b** Configuration-averaged two-terminal conductance G at $t_2 = 0$. Inset displays the averaged spectral gap and inverse participation ratio for $L = 90$ as a function of M. $(t_2, M^c) = (0, 1.1)$ and $(t_2, M^c) = (0, 2.9)$ denote the gapped-gapless transition points, with the gapless region hosting localized states.

random fractal phase, the energy gap closes and remains closed in the topological and Anderson insulator phases. Despite being gapless, and in contrast to the studies of deterministic fractals[50,55,57], we uncover unambiguous and robust quantization of conductance in the topological random fractal phase. The formation of the quantized plateau as a function of finite t_2 is demonstrated in Fig. 4(b). At the tricritical point $(t_2^c, M^c) \approx (0, 1.1)$, even a marginal increase of t_2 leads to formation of the topological phase with robust conductance quantization. In Fig. 4(c), we have plotted the conductance as a function of the energy (or the chemical potential of the leads) for a number of individual random fractal realizations. All the samples exhibit a finite quantized plateau around $E = 0$. While the topological random fractal phase is gapless, the topology is protected by a mobility gap. The width of the plateaus in Fig. 4(c), which show sample-to-sample fluctuations, corresponds to the value of the mobility gap. As long as the energy is located in the mobility gap, the conductance (for samples larger than the localization length) remains quantized.

As a testament to the remarkable robustness of the topological states, as the system size grows, the conductance quantization becomes accurate despite the great complexity and variation of different random fractal realizations. As illustrated by histograms in Fig. 4(d), well inside the topological regime, over 90% of configurations with the linear size $L = 1600$ display conductance quantization with 1% accuracy or better. As seen in Fig. 4(e), the quantization develops rapidly when moving from the tricritical point towards the topological phase. Larger systems exhibit on average more precise quantization, indicating that the random fractal phase is a well-defined thermodynamic phase of matter.

To illustrate that topological random fractals constitute a well-defined thermodynamic phase of matter, we carry out a finite-size scaling study. According to the theory of topological localization transitions, near the transition one expects that the configuration-averaged conductance obeys a single-parameter scaling hypothesis in the large system limit. This hypothesis predicts that the conductance curves for different system sizes collapse to a universal curve $G = f\left[L^{1/\nu}\zeta\right]$, where ζ represents a parameter that drives the transition[85]. The scaling function f approaches 0 (1) at large negative (positive) arguments. The scaling behaviour indicates that the system undergoes a sharply-defined topological phase transition at $\zeta = 0$ in the thermodynamic limit, separating two distinct phases of matter. The localization length critical exponent ν is expected to be universal for all systems with the same spatial dimension and symmetry class. In particular, for symmetry class D in two dimensions the exponent is $\nu = 1$[79,80]. A high-precision determination of the critical exponents in the topological random fractal is beyond the scope of the present work. However, by calculating the conductance as a function of the second-nearest-neighbour hopping, to explore the validity of the scaling hypothesis $G = f\left[L^{1/\nu}(t_2 - t_2^c)\right]$, we can show that the standard two-dimensional class D scaling does not match the numerical evidence. In Fig. 5(a), we employ the value $\nu = 1$ expected for the insulator-insulator phase transition for class D systems in two dimensions. The curves do accurately cross in a single point, indicating that sufficiently close to the critical point, the system sizes $L = 300 - 1100$ are in the single-parameter scaling regime, but the data clearly do not follow a single curve. As a contrast, as seen in Fig. 5(b) for a higher value exponent $\nu = 2.4$, the curves collapse to a single curve near the critical point. While not yielding a high-precision numerical value for the exponent, the data supports the conclusion that the transition obeys scaling behaviour. The observed substantial departure of the critical exponent from its universal 2d value further suggests that, despite bearing similarities to its integer-dimensional counterpart, the random fractal phase is a genuinely distinct phase of matter with unique critical properties. Additionally, as the curves are accurate near the critical point we can extract the critical conductance $G^c \approx 0.65$, which provides the basis for the white dashed line as an approximate phase boundary in Fig. 2.

Discussion

In this work we introduced an electronic state of matter, topological random fractals, and established its central properties. The studied system, supporting robust quantized conductance protected by a mobility gap, constitutes of the first example of a non-integer-dimensional system defined on a random lattice and, in this sense, is the most complex realization of nontrivial band topology known to date. The finite-size scaling results suggest that the topological random fractals belong to a different universality class than their integer-dimensional parent states, calling for further studies on topological fractals. Besides the fundamental interest, there is reason for optimism that such systems will become available for experimental studies in the near future. Technological advances have enabled fabrication of artificial and quantum simulator systems realizing quasicrystalline and fractal electronic

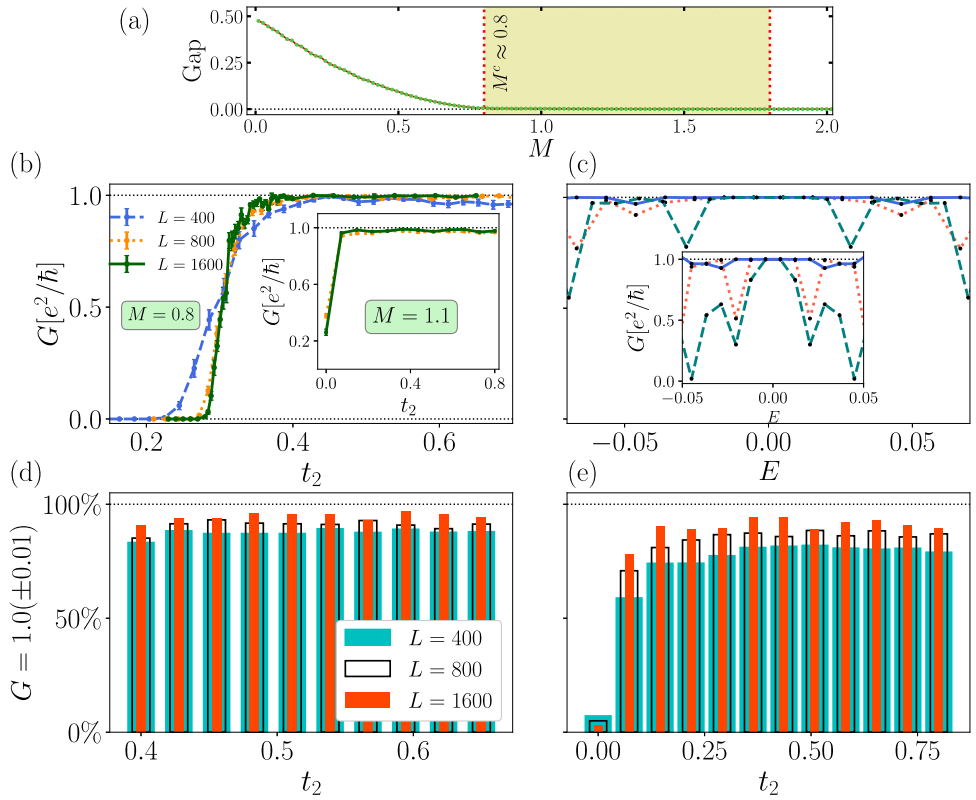

Fig. 4 Properties of topological random fractal phase. a The average spectral gap above the ground state as a function of the mass parameter M with linear system size $L = 100$ and second-nearest-neighbour hopping $t_2 = 0.3$. The gapped-gapless phase transition coincides with the trivial-topological fractal transition at $M^c \approx 0.8$. The average is taken over 150 random configurations and the error bars (not shown) are of the order of 10^{-3}. **b** Two-terminal conductance G as a function of t_2 at $(E, M) = (0, 0.8)$ signifying the transition from a spectral insulator to a topological random fractal phase. E indicates the energy at which the conductance is calculated. (Inset) Same for $(E, M) = (0, 1.1)$. **c** Conductance for different individual realizations of topological random fractals as a function of energy for $(t_2, M) = (0.45, 0.8)$ and (inset) $(t_2, M) = (0.25, 1.1)$ for $L = 1600$. **d** Percentage of the samples falling into 1% of the quantization range for $(E, M) = (0, 0.8)$. **e** Same as (**d**) for $(E, M) = (0, 1.1)$. Panels (**d**) and (**e**) are calculated for roughly 10^3 independent samples at each point.

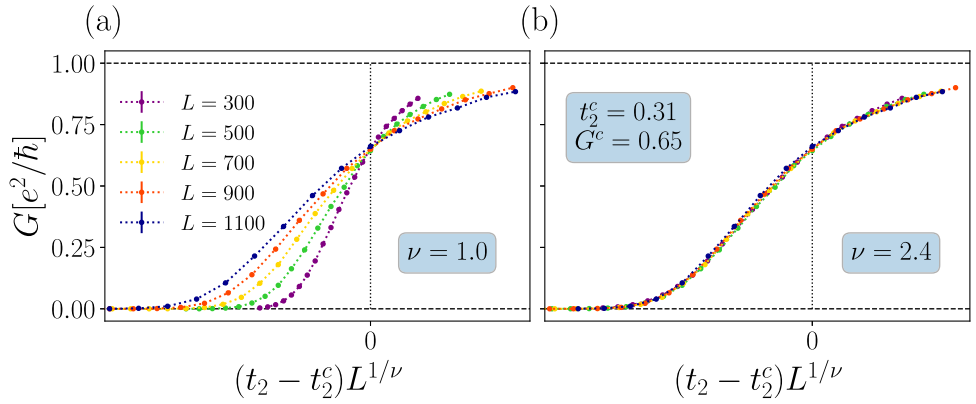

Fig. 5 Finite-size scaling of conductance for half-filled systems. a Conductance data fit at the mass parameter $M = 0.8$ with the 2d class D exponent $\nu = 1$, which fails to capture the correct scaling behaviour. In contrast, with the localization exponent $\nu = 2.4$ in **b** the data collapse to a universal curve. Curves are averaged over $10^3 - 10^4$ distinct random fractal configurations at each data point.

structures[46,48,49]. These advances suggest that experimental realization of topological random fractals may not be far behind.

Methods

Generating random fractals. We construct the studied random lattices by starting with an $L \times L$ square lattice, and independently associating a probability $p = p_c \approx 0.5927$ for each site being populated. After drawing the random populations of all sites from a uniform distribution, we keep a single remaining cluster which connects the left and right edges of the lattice (statistically present in half of the end configurations). To this cluster we associate the Hamiltonian of Eq. (1), modified appropriately by the missing sites and hoppings; in the clean limit this would be a topologically nontrivial system as seen in Fig. 6. Repeating this process many times provides us with a statistical sample of $10^3 - 10^4$ finite snapshots of infinite random fractal lattices.

Calculation of two-terminal conductance. We employ the KWANT software[83] to extract the two-terminal conductances. The obtained $L \times L$ random fractal configurations are attached to two identical semi-infinite metallic leads, represented by a set of parallel decoupled 1d chains. As seen in Fig. 7 for a square lattice with leads

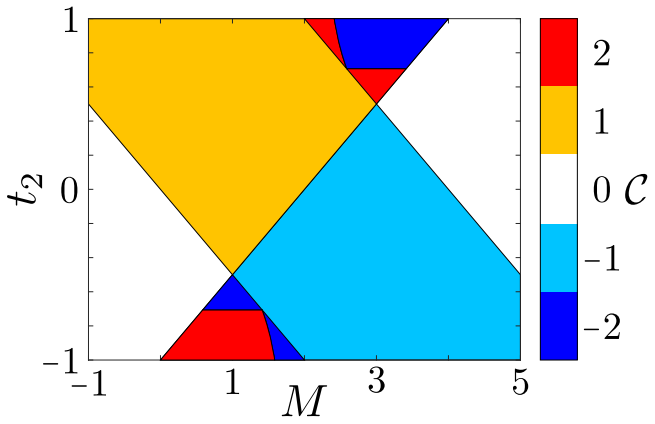

Fig. 6 Chern numbers of a defect-free system. The figure corresponds to the Hamiltonian in Eq. (1) with occupation probability $p = 1$, the mass parameter M and the second-nearest-neighbour hopping t_2. Colour bar indicates the value of the Chern number $\mathcal{C}$.

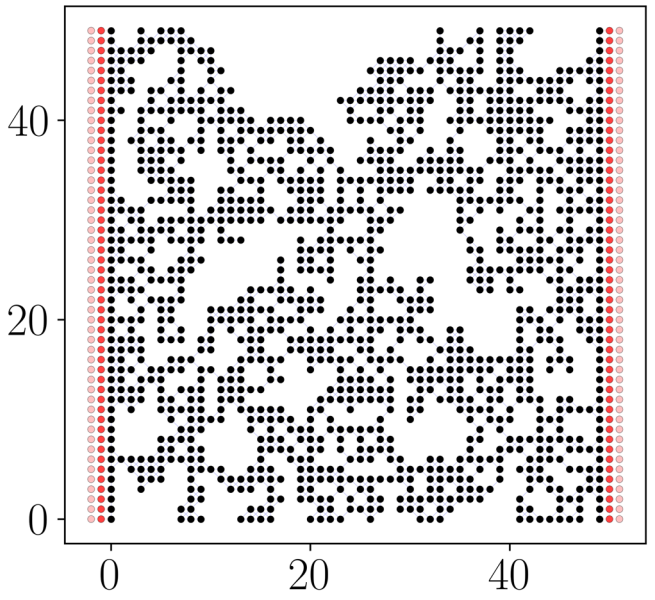

Fig. 7 Transport setup. Here we see a random snapshot of a 50×50 system and its leads connectivity. In order to ensure the full lead-system connectivity, a row of lattice sites are appended at each ends.

attached in y-direction, the repeating unit cell is a vertical line of points, such that the open tight-binding chain along y gets repeated in x-direction. We employ large-scale parallel computing to carry out the calculation of the configuration-averaged conductance of up to 10^4 different random configurations per parameter point for linear system sizes $L = 120-1600$.

Data availability

The data supporting the findings of this work are available upon reasonable request.

Code availability

The codes implementing the calculations in this work are available upon reasonable request.

Received: 25 February 2022; Accepted: 22 November 2022;
Published online: 14 December 2022

References

1. Klitzing, K. V., Dorda, G. & Pepper, M. New method for high-accuracy determination of the fine-structure constant based on quantized Hall resistance. *Phys. Rev. Lett.* **45**, 494–497 (1980).
2. Thouless, D. J., Kohmoto, M., Nightingale, M. P. & den Nijs, M. Quantized Hall conductance in a two-dimensional periodic potential. *Phys. Rev. Lett.* **49**, 405–408 (1982).
3. Laughlin, R. B. Quantized Hall conductivity in two dimensions. *Phys. Rev. B* **23**, 5632–5633 (1981).
4. Hatsugai, Y. Chern number and edge states in the integer quantum Hall effect. *Phys. Rev. Lett.* **71**, 3697–3700 (1993).
5. Qi, X.-L. & Zhang, S.-C. Topological insulators and superconductors. *Rev. Mod. Phys.* **83**, 1057–1110 (2011).
6. Vergniory, M. et al. A complete catalogue of high-quality topological materials. *Nature* **566**, 480–485 (2019).
7. Zhang, T. et al. Catalogue of topological electronic materials. *Nature* **566**, 475–479 (2019).
8. Tang, F., Po, H. C., Vishwanath, A. & Wan, X. Comprehensive search for topological materials using symmetry indicators. *Nature* **566**, 486–489 (2019).
9. Zhou, P. et al. Photonic amorphous topological insulator. *Light Sci. Appl.* **9**, 133 (2020).
10. Corbae, P. et al. Evidence for topological surface states in amorphous Bi_2Se_3. arXiv preprint at https://arxiv.org/abs/1910.13412v2 (2019).
11. Mitchell, N. P., Nash, L. M., Hexner, D., Turner, A. M. & Irvine, W. T. Amorphous topological insulators constructed from random point sets. *Nat. Phys.* **14**, 380–385 (2018).
12. Fulga, I. C., Pikulin, D. I. & Loring, T. A. Aperiodic weak topological superconductors. *Phys. Rev. Lett.* 116, 257002 (2016).
13. Agarwala, A. & Shenoy, V. B. Topological insulators in amorphous systems. *Phys. Rev. Lett.* **118**, 236402 (2017).
14. Yang, Y.-B., Qin, T., Deng, D.-L., Duan, L.-M. & Xu, Y. Topological amorphous metals. *Phys. Rev. Lett.* **123**, 076401 (2019).
15. Costa, M., Schleder, G. R., Buongiorno Nardelli, M., Lewenkopf, C. & Fazzio, A. Toward realistic amorphous topological insulators. *Nano Lett.* **19**, 8941–8946 (2019).
16. Huang, H. & Liu, F. Quantum spin Hall effect and spin bott index in a quasicrystal lattice. *Phys. Rev. Lett.* **121**, 126401 (2018).
17. Varjas, D. et al. Topological phases without crystalline counterparts. *Phys. Rev. Lett.* **123**, 196401 (2019).
18. Mukati, P., Agarwala, A. & Bhattacharjee, S. Topological and conventional phases of a three-dimensional electronic glass. *Phys. Rev. B* **101**, 035142 (2020).
19. Agarwala, A., Juričić, V. & Roy, B. Higher-order topological insulators in amorphous solids. *Phys. Rev. Res.* **2**, 012067 (2020).
20. Mitchell, N. P., Turner, A. M. & Irvine, W. T. M. Real-space origin of topological band gaps, localization, and reentrant phase transitions in gyroscopic metamaterials. *Phys. Rev. E* **104**, 025007 (2021).
21. Kraus, Y. E., Lahini, Y., Ringel, Z., Verbin, M. & Zilberberg, O. Topological states and adiabatic pumping in quasicrystals. *Phys. Rev. Lett.* **109**, 106402 (2012).
22. Araújo, R. N. & Andrade, E. C. Conventional superconductivity in quasicrystals. *Phys. Rev. B* **100**, 014510 (2019).
23. Chen, R., Chen, C.-Z., Gao, J.-H., Zhou, B. & Xu, D.-H. Higher-order topological insulators in quasicrystals. *Phys. Rev. Lett.* **124**, 036803 (2020).
24. Kraus, Y. E., Ringel, Z. & Zilberberg, O. Four-dimensional quantum Hall effect in a two-dimensional quasicrystal. *Phys. Rev. Lett.* **111**, 226401 (2013).
25. Pöyhönen, K., Sahlberg, I., Weststrom, A. & Ojanen, T. Amorphous topological superconductivity in a Shiba glass. *Nat. Commun.* **9**, 2103 (2018).
26. Xiao, M. & Fan, S. Photonic chern insulator through homogenization of an array of particles. *Phys. Rev. B* **96**, 100202 (2017).
27. Mano, T. & Ohtsuki, T. Application of convolutional neural network to quantum percolation in topological insulators. *J. Phys. Soc. Jpn* **88**, 123704 (2019).
28. Sahlberg, I., Weststrom, A., Pöyhönen, K. & Ojanen, T. Topological phase transitions in glassy quantum matter. *Phys. Rev. Res.* **2**, 013053 (2020).
29. Marsal, Q., Varjas, D. & Grushin, A. G. Topological Weaire–Thorpe models of amorphous matter. *Proc. Natl Acad. Sci. USA* **117**, 30260–30265 (2020).
30. Grushin, A. G. Topological Phases of Amorphous Matter. Low-Temperature Thermal and Vibrational Properties of Disordered Solids, 435–486 (World Scientific, 2022).
31. Focassio, B., Schleder, G. R., Crasto de Lima, F., Lewenkopf, C. & Fazzio, A. Amorphous Bi_2Se_3 structural, electronic, and topological nature from first principles. *Phys. Rev. B* **104**, 214206 (2021).
32. Bandres, M. A., Rechtsman, M. C. & Segev, M. Topological photonic quasicrystals: Fractal topological spectrum and protected transport. *Phys. Rev. X* **6**, 011016 (2016).

33. Ivaki, M. N., Sahlberg, I. & Ojanen, T. Criticality in amorphous topological matter: Beyond the universal scaling paradigm. *Phys. Rev. Res.* **2**, 043301 (2020).
34. Zhou, D., Zhang, L. & Mao, X. Topological boundary floppy modes in quasicrystals. *Phys. Rev. X* **9**, 021054 (2019).
35. Loring, T. A. Bulk spectrum and k-theory for infinite-area topological quasicrystals. *Journal of Mathematical Physics* **60**, 081903 (2019).
36. Corbae, P., Hellman, F. & Griffin, S. M. Structural disorder-driven topological phase transition in noncentrosymmetric BiTeI. *Phys. Rev. B* **103**, 214203 (2021).
37. Verbin, M., Zilberberg, O., Kraus, Y. E., Lahini, Y. & Silberberg, Y. Observation of topological phase transitions in photonic quasicrystals. *Phys. Rev. Lett.* **110**, 076403 (2013).
38. Hua, C.-B., Chen, R., Zhou, B. & Xu, D.-H. Higher-order topological insulator in a dodecagonal quasicrystal. *Phys. Rev. B* **102**, 241102 (2020).
39. Li, K., Wang, J.-H., Yang, Y.-B. & Xu, Y. Symmetry-protected topological phases in a rydberg glass. *Phys. Rev. Lett.* **127**, 263004 (2021).
40. Wang, J.-H., Yang, Y.-B., Dai, N. & Xu, Y. Structural-disorder-induced second-order topological insulators in three dimensions. *Phys. Rev. Lett.* **126**, 206404 (2021).
41. Spring, H., Akhmerov, A. R. & Varjas, D. Amorphous topological phases protected by continuous rotation symmetry. *SciPost Phys.* **11**, 22 (2021).
42. Else, D. V., Huang, S.-J., Prem, A. & Gromov, A. Quantum many-body topology of quasicrystals. *Phys. Rev. X* **11**, 041051 (2021).
43. Lv, B. et al. Realization of quasicrystalline quadrupole topological insulators in electrical circuits. *Commun. Phys.* **4**, 1–6 (2021).
44. Khajetoorians, A. A., Wegner, D., Otte, A. F. & Swart, I. Creating designer quantum states of matter atom-by-atom. *Nat. Rev. Phys.* **1**, 703–715 (2019).
45. Drost, R., Ojanen, T., Harju, A. & Liljeroth, P. Topological states in engineered atomic lattices. *Nat. Phys.* **13**, 668–671 (2017).
46. Kempkes, S. N. et al. Design and characterization of electrons in a fractal geometry. *Nat. Phys.* **15**, 127–131 (2019).
47. Dong, J., Juričić, V. & Roy, B. Topolectric circuits: theory and construction. *Phys. Rev. Res.* **3**, 023056 (2021).
48. Liu, C. et al. Sierpiński structure and electronic topology in bi thin films on insb(111)b surfaces. *Phys. Rev. Lett.* **126**, 176102 (2021).
49. Shang, J. et al. Assembling molecular sierpiński triangle fractals. *Nat. Chem.* **7**, 389–393 (2015).
50. Fischer, S. et al. Robustness of chiral edge modes in fractal-like lattices below two dimensions: a case study. *Phys. Rev. Res.* **3**, 043103 (2021).
51. Fremling, M., van Hooft, M., Smith, C. M. & Fritz, L. Existence of robust edge currents in Sierpiński fractals. *Phys. Rev. Res.* **2**, 013044 (2020).
52. Sarangi, S. & Nielsen, A. E. B. Effect of coordination on topological phases on self-similar structures. *Phys. Rev. B* **104**, 045147 (2021).
53. Pai, S. & Prem, A. Topological states on fractal lattices. *Phys. Rev. B* **100**, 155135 (2019).
54. Manna, S., Pal, B., Wang, W. & Nielsen, A. E. B. Anyons and fractional quantum Hall effect in fractal dimensions. *Phys. Rev. Res.* **2**, 023401 (2020).
55. Iliasov, A. A., Katsnelson, M. I. & Yuan, S. Hall conductivity of a Sierpiński carpet. *Phys. Rev. B* **101**, 045413 (2020).
56. Brzezińska, M., Cook, A. M. & Neupert, T. Topology in the Sierpiński-Hofstadter problem. *Phys. Rev. B* **98**, 205116 (2018).
57. Agarwala, A., Pai, S. & Shenoy, V. B. Fractalized metals. Preprint at https://arxiv.org/abs/1803.01404 (2018).
58. Song, Z.-G., Zhang, Y.-Y. & Li, S.-S. The topological insulator in a fractal space. *Appl. Phys. Lett.* **104**, 233106 (2014).
59. Manna, S., Duncan, C. W., Weidner, C. A., Sherson, J. F. & Nielsen, A. E. B. Anyon braiding on a fractal lattice with a local hamiltonian. *Phys. Rev. A* **105**, L021302 (2022).
60. Manna, S., Nandy, S. & Roy, B. Higher-order topological phases on fractal lattices. *Phys. Rev. B.* **105**, L201301 (2022).
61. Manna, S., Jaworowski, B. & Nielsen, A. E. Many-body localization on finite generation fractal lattices. Preprint at https://arxiv.org/pdf/2111.13516.pdf (2021).
62. Yang, Z., Lustig, E., Lumer, Y. & Segev, M. Photonic floquet topological insulators in a fractal lattice. *Light Sci. Appl.* **9**, 1–7 (2020).
63. Nakayama, T. & Yakubo, K. *Fractal Concepts in Condensed Matter Physics*, vol. 140 (Springer Science & Business Media, 2003).
64. Kosior, A. & Sacha, K. Localization in random fractal lattices. *Phys. Rev. B* **95**, 104206 (2017).
65. Stauffer, D. & Aharony, A. *Introduction to Percolation Theory* (CRC Press, 2018).
66. Isichenko, M. B. Percolation, statistical topography, and transport in random media. *Rev. Mod. Phys.* **64**, 961–1043 (1992).
67. Nakayama, T., Yakubo, K. & Orbach, R. L. Dynamical properties of fractal networks: Scaling, numerical simulations, and physical realizations. *Rev. Mod. Phys.* **66**, 381–443 (1994).
68. Albert, R. & Barabási, A.-L. Statistical mechanics of complex networks. *Rev. Mod. Phys.* **74**, 47–97 (2002).
69. Qi, X.-L., Wu, Y.-S. & Zhang, S.-C. Topological quantization of the spin Hall effect in two-dimensional paramagnetic semiconductors. *Phys. Rev. B* **74**, 085308 (2006).
70. Asbóth, J. K., Oroszlány, L. & Pályi, A. *Two-Dimensional Chern Insulators: the Qi-Wu-Zhang Model*, 85–98 (Springer International Publishing, Cham, 2016).
71. Wu, H. C., Jin, L. & Song, Z. Nontrivial topological phase with a zero Chern number. *Phys. Rev. B* **102**, 035145 (2020).
72. Altland, A. & Zirnbauer, M. R. Nonstandard symmetry classes in mesoscopic normal-superconducting hybrid structures. *Phys. Rev. B* **55**, 1142–1161 (1997).
73. Chiu, C.-K., Teo, J. C. Y., Schnyder, A. P. & Ryu, S. Classification of topological quantum matter with symmetries. *Rev. Mod. Phys.* **88**, 035005 (2016).
74. Evers, F. & Mirlin, A. D. Anderson transitions. *Rev. Mod. Phys.* **80**, 1355–1417 (2008).
75. Medvedyeva, M. V., Tworzydło, J. & Beenakker, C. W. J. Effective mass and tricritical point for lattice fermions localized by a random mass. *Phys. Rev. B* **81**, 214203 (2010).
76. Wimmer, M., Akhmerov, A. R., Medvedyeva, M. V., Tworzydło, J. & Beenakker, C. W. J. Majorana bound states without vortices in topological superconductors with electrostatic defects. *Phys. Rev. Lett.* **105**, 046803 (2010).
77. Kagalovsky, V. & Nemirovsky, D. Universal critical exponent in class D superconductors. *Phys. Rev. Lett.* **101**, 127001 (2008).
78. Chalker, J. T. et al. Thermal metal in network models of a disordered two-dimensional superconductor. *Phys. Rev. B* **65**, 012506 (2001).
79. Wang, T., Pan, Z., Ohtsuki, T., Gruzberg, I. A. & Shindou, R. Multicriticality of two-dimensional class-D disordered topological superconductors. *Phys. Rev. B* **104**, 184201 (2021).
80. Pan, Z., Wang, T., Ohtsuki, T. & Shindou, R. Renormalization group analysis of Dirac fermions with a random mass. *Phys. Rev. B* **104**, 174205 (2021).
81. Li, X., Jha, M. C. & Nielsen, A. E. Laughlin topology on fractal lattices without area law entanglement. *Phys. Rev. B* **105**, 085152 (2022).
82. Iliasov, A. A., Katsnelson, M. I. & Yuan, S. Power-law energy level spacing distributions in fractals. *Phys. Rev. B* **99**, 075402 (2019).
83. Groth, C. W., Wimmer, M., Akhmerov, A. R. & Waintal, X. Kwant: a software package for quantum transport. *New J. Phys.* **16**, 063065 (2014).
84. Beenakker, C. W. J. Random-matrix theory of quantum transport. *Rev. Mod. Phys.* **69**, 731–808 (1997).
85. Huckestein, B. Scaling theory of the integer quantum Hall effect. *Rev. Mod. Phys.* **67**, 357 (1995).

Acknowledgements

The authors acknowledge the Academy of Finland project 331094 for support.

Author contributions

The project was planned jointly by M.I., I.S., K.P., and T.O. The numerical calculations were carried out by M.I. with some assistance from I.S. All the authors participated in analyzing the results, discussing their interpretation and writing the manuscript.

Competing interests

The authors declare no competing interests.

Additional information

Supplementary information The online version contains supplementary material available at https://doi.org/10.1038/s42005-022-01101-z.

Correspondence and requests for materials should be addressed to Teemu Ojanen.

Peer review information *Communications Physics* thanks Mikael Fremling and the other, anonymous, reviewer(s) for their contribution to the peer review of this work. Peer reviewer reports are available.

Reprints and permission information is available at http://www.nature.com/reprints

Publisher's note Springer Nature remains neutral with regard to jurisdictional claims in published maps and institutional affiliations.